11th International Symposium on Turbulence and Shear Flow Phenomena (TSFP11)
Southampton, UK, July 30 to August 2, 2019

REDUCED-ORDER MODELS TO ANALYSE COHERENT STRUCTURES IN TURBULENT PIPE FLOW

Leandra I. Abreu
Department of Aeronautical Engineering
Instituto Tecnológico de Aeronáutica
12228-900, São José dos Campos, SP, Brazil
leandraabreu13@gmail.com

André V. G. Cavalieri
Department of Aeronautical Engineering
Instituto Tecnológico de Aeronáutica
12228-900, São José dos Campos, SP, Brazil
andre@ita.br

Philipp Schlatter
Department of Mechanics
KTH Royal Institute of Technology
SE-100-44, Stockholm, Sweden
pschlatt@mech.kth.se

Ricardo Vinuesa
Department of Mechanics
KTH Royal Institute of Technology
SE-100-44, Stockholm, Sweden
rvinuesa@mech.kth.se

Dan Henningson
Department of Mechanics
KTH Royal Institute of Technology
SE-100-44, Stockholm, Sweden
henning@mech.kth.se

ABSTRACT

Fully resolved direct numerical simulations, performed with a high-order spectral-element method, are used to study coherent structures in turbulent pipe flow at friction Reynolds numbers $Re_\tau = 180$ and 550 (El Khoury *et al.*, 2013). The database was analysed using spectral proper orthogonal decomposition (SPOD) so as to identify dominant coherent structures, most of which are of streaky shape. As a reduced-order model for such structures, the linearised flow response to harmonic forcing was computed, and the analysed singular modes of the resolvent operator were analysed. For turbulent flows, this approach amounts to considering the non-linear terms in the Navier–Stokes system as an unknown forcing, treated convenienty as external. Resolvent analysis then allows an identification of the optimal forcing and most amplified flow response; the latter may be related to observed relevant structures obtained by SPOD, especially if the gain between forcing and response is much larger than what is found for suboptimal forcings or if the non-linear forcing is white noise. Results from SPOD and resolvent analysis were extracted for several combinations of frequencies, streamwise and azimuthal wavenumbers. For both Reynolds numbers, good agreement between SPOD and resolvent modes was observed for parameter combinations where the lift-up mechanism is present: optimal forcing from resolvent analysis represents streamwise vortices and the associated response are streaky structures.

INTRODUCTION

In turbulent wall-bounded flows, such as pipes, channels and boundary layers, near-wall streaks are the most typically observed coherent structures, they are extremely relevant near-wall structures in wall-bounded turbulence (Kline *et al.*, 1967; Gupta *et al.*, 1971). Such streaky structures are regions of alternating low and high momentum located in the viscous and buffer layers with a characteristic spanwise spacing of $100\nu/u_\tau$, where u_τ is the friction velocity and ν is the kinematic viscosity of the fluid (Marusic *et al.*, 2017). For higher wall-normal positions, larger structures are observed, with similar streaky shape (Marusic *et al.*, 2017). The study of a turbulent flow along the surface of a solid body and its interaction with the wall is one of the most fundamental problems in fluid mechanics. Thus, the pursuit for more effective methods to model and characterize near-wall coherent structures is a very relevant problem.

For that matter, the use of statistical methods in flow databases can be convenient to identify coherent structures present in the flow. Certain turbulence statistics, taken in frequency and wavenumber domain whenever possible, can be optimally represented using a spectral proper orthogonal decomposition (SPOD), this method involves decomposition of the cross-spectral density tensor (CSD) and leads to modes oscillating at a specific frequency (Towne *et al.*, 2018). The leading SPOD modes show the most likely spatial structures that arise in turbulent-flow realisations, sorted in terms of their contribution to the overall power; SPOD is thus a useful method to extract energetic coherent structures in turbulence.

Recent works have explored the connection of SPOD modes with the flow responses to stochastic forcing (Abreu *et al.*, 2017, see for instance); note that such responses are obtained using the linearised resolvent operator, consider-

ing the mean field as base flow for linearisation. In this context, the non-linear fluctuation terms are treated as an external forcing (McKeon & Sharma, 2010; Gómez *et al.*, 2014). These linearised responses can often be related to results of hydrodynamic stability theory, with modes corresponding to linear stability eigenfunctions or to non-modal mechanisms such as lift-up (Jovanovic & Bamieh, 2005), but in recent years resolvent analysis has been used to study coherent structures in turbulent flows (see the review of (McKeon, 2017) and references therein). An important result is that if the forcing can be modeled as spatial white noise, a direct correspondence between SPOD and resolvent modes is expected (Towne *et al.*, 2018). Moreover, for a flow with a dominant optimal forcing, leading to a gain much larger than that of suboptimal ones, the CSD will often be dominated by the leading response obtained in resolvent analysis (Cavalieri *et al.*, 2019).

Thus a combined analysis of the flow, with SPOD serving to decompose turbulent fluctuations and resolvent analysis as a theoretical framework, enables a reduced-order model of the dynamically-relevant flow features. A number of previous studies works have dealt with POD (without frequency decomposition) (Hellström *et al.*, 2016) and resolvent analysis (McKeon & Sharma, 2010) for turbulent pipe flow, but the ability of the latter to model SPOD modes has not been addressed by a thorough comparison involving the range of relevant wavenumbers and frequencies. This is pursued here for turbulent pipe flow, a canonical configuration for the study of wall-bounded turbulence.

In the present study, we apply SPOD to turbulent pipe flow, following the approach outlined by Towne *et al.* (2018), with the standard incompressible turbulent kinetic energy norm. We take a Fourier decomposition of velocity fields in all homogeneous directions: streamwise, azimuthal directions and time, so then we obtain the field for specifics wavenumbers, k_x and k_z, and frequency ω, *i.e.* $\hat{\mathbf{q}}(k_x, r, k_z, \omega)$, where hats denote Fourier-transformed quantities; we then apply the SPOD to this transformed field, which is equivalent to solving the integral equation:

$$\int \mathbf{C}(\mathbf{r}, \mathbf{r}', \omega)\Psi(\mathbf{r}', \omega)d\mathbf{r}' = \lambda(\omega)\Psi(\mathbf{r}, \omega), \qquad (1)$$

where Ψ are the basis functions, also called SPOD modes, λ is the corresponding eigenvalue and $\mathbf{C}$ is the two-point cross-spectral density. $\mathbf{C}$ is a Hermitian matrix, and thus its eigenvalues are real and the eigenfunctions are orthogonal.

To perform the resolvent analysis we follow the formulation described by McKeon & Sharma (2010) for a pipe flow with a smaller Reynolds numbers. The Navier-Stokes system can be written in operator notation as

$$\hat{\mathbf{q}} = (i\omega\mathbf{I} - \mathscr{L})^{-1}\hat{\mathbf{f}}, \qquad (2)$$

where $\mathscr{L}$ is the linearised Navier-Stokes operator considering the mean profile $U(r)$ as a base flow, and all variables are Fourier transformed in time, axial and azimuthal directions. The resolvent operator is $\mathscr{R} = (i\omega\mathbf{I} - \mathscr{L})^{-1}$, and its singular value decomposition leads to optimal forcing modes, leading to maximum amplification of corresponding flow responses. More details about the present formulation can be seen in McKeon & Sharma (2010).

DNS databases were taken from the work of El Khoury *et al.* (2013) and further information can be find in that paper.

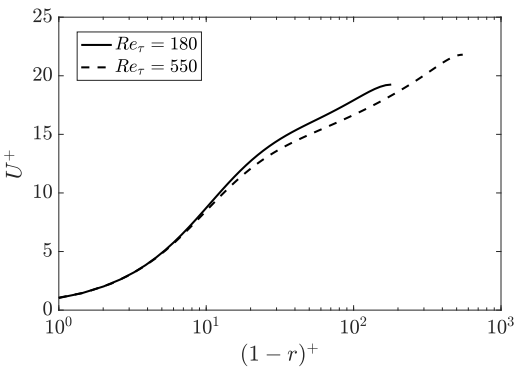

(a)

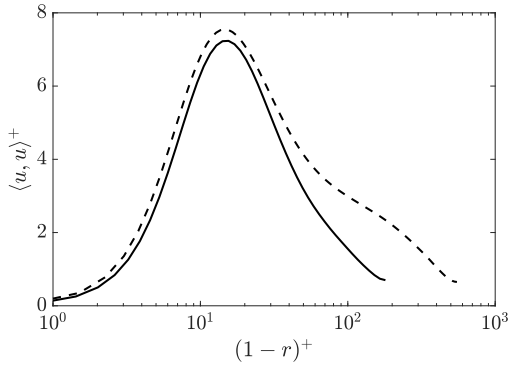

(b)

Figure 1. (a) The mean flow and (b) streamwise velocity fluctuations at $Re_\tau = 180$ (black solid line) and 550 (black dashed line), both scaled in viscous units.

TURBULENCE STATISTICS AND SPECTRA

The mean streamwise velocity profiles (U^+) and the variance profile of streamwise velocity fluctuations ($\langle u, u\rangle^+$) in inner scaling are shown in Figures 1 (a) and (b) respectively, for $Re_\tau = 180$ and 550, where $Re_\tau = R^+$ is the friction Reynolds number. Here U is mean quantities and u fluctuating. The inner scaling is defined by the friction velocity u_τ, and the length by the viscous length scale ν/u_τ and the superscript $+$. The mean velocity profiles show the expected shape of wall-bounded turbulent flows when plotted as a function of wall distance in inner scaling $(1-r)^+$, where r is the radial coordinate, starting at the pipe center. Variance profiles also have the expected pattern characteristic of wall-blinded turbulent flows, with a near-wall peak in the buffer layer at $(1-r)^+ \approx 15$, which increases its magnitude for the higer Reynolds number.

In order to visualize turbulent structures present in the buffer layer, Figures 2 (a) and (b) show snapshots of streamwise velocity fluctuations (u/u_τ) in wall-parallel stations at $(1-r)^+ \approx 15$, for $Re_\tau = 180$ and 550. The dominant structures have the characteristic streaky shape, elongated in the streamwise direction x in all cases. The buffer-layer streaks, typical structures located at $(1-r)^+ = 15$, have a characteristic azimuthal wavelength of $\lambda_z^+ = r^+\lambda_\theta \approx 100$, as expected. These features are standard in wall-bounded turbulent flows (Marusic *et al.*, 2017; Kline *et al.*, 1967; Gupta *et al.*, 1971, see for instance). In what follows we will use $z^+ = r^+\theta$ as a pseudo-spanwise coordinate for simple comparison with results for boundary layers and channels.

The 2D inner-scaled premultiplied power-spectral density of streamwise velocity fluctuations $k_x^+ k_z^+ E_{uu}^+$ are shown

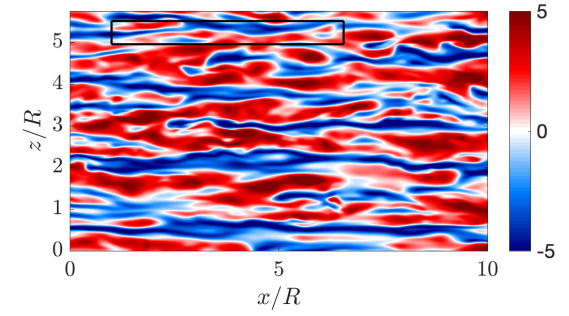

(a) $Re_\tau = 180$

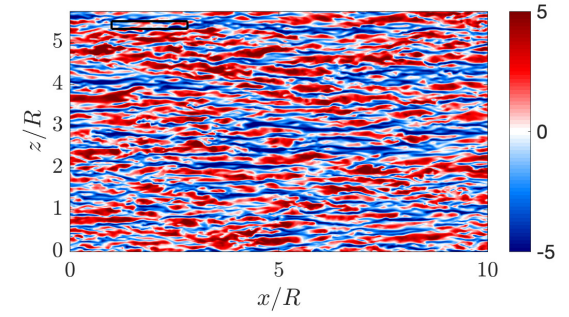

(b) $Re_\tau = 550$

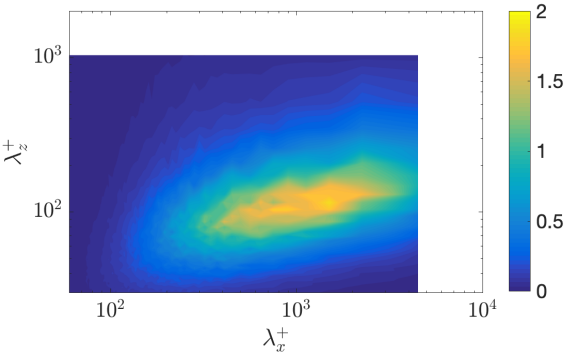

(c) $Re_\tau = 180$

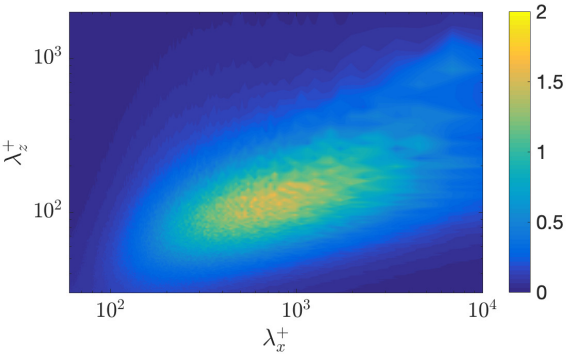

(d) $Re_\tau = 550$

Figure 2. Results in the buffer layer $(1-r)^+ \approx 15$ for both $Re_\tau = 180$ and 550; (a,b) show instantaneous streamwise velocity fluctuation (u^+) field in the wall-parallel plane, where the black rectangle here represents $(\lambda_x^+, \lambda_z^+) \approx (1000, 100)$; and (c,d) show the 2D inner-scaled premultiplied power-spectral density of the streamwise velocity $k_x^+ k_z^+ E_{uu}^+$.

in Figures 2 (c) and (d) at $(1-r)^+ \approx 15$ for $Re_\tau = 180$ and 550, respectively. Note that k_x^+ and k_z^+ refer respectively to streamwise and azimuthal wavenumbers. The wavelength combination corresponding to $(\lambda_x^+, \lambda_z^+) \approx (1000, 100)$ is representative of the signature of the near-wall cycle in many studies across a range of Reynolds numbers and flow types (Hoyas & Jiménez, 2006), as we can observe for both analysed friction Reynolds numbers in Figures 2 (c) and (d). This peak is due to the near-wall cycle of streaks and quasi-streamwise vortices (Jiménez, 2013). At high Reynolds numbers, there is also an appearance of a second peak in the outer region of the flow, corresponding to very large scale motions or superstructures (Monty *et al.*, 2009). Here we can identify this second spectral peak starting to appear at $Re_\tau = 550$ for $\lambda_z^+ \approx 840$ and $\lambda_x^+ \approx 7000$.

In the present study we are investigating streaky strutures, which are elongated structures in the streamwise direction, where $\lambda_x^+ \gg \lambda_z^+$ (or $k_x^+ \ll k_z^+$), also with low characteristic frequency. Visualisations and spectra in Figure 2 show that these are dominant structures in the buffer layer of turbulent pipe flow.

RESULTS AND DISCUSSION

Comparison between SPOD and resolvent modes

Figure 3 shows the first SPOD mode compared with the optimal response from resolvent analysis at $Re_\tau = 550$ considering $(\lambda_x^+, \lambda_z^+, \lambda_t^+) \approx (1000, 100, 100)$, or correspondent frequency $\omega+ = 2\pi/\lambda_t^+ \approx 0.06$, which is representative of the near-wall cycle. Notice that the vertical direction does not correspond to constant spacing in viscous length scale, due to polar system. We can see in all results the dominance of streaky structures and streamwise vortices, as expected, since in the near-wall region the predominant structures are low-speed and high-speed streaks which are generated by streamwise vortices (Hamilton *et al.*, 1995; Jiménez, 2013). Similar results were obtained for $Re_\tau = 180$ at $(\lambda_x^+, \lambda_z^+, \lambda_t^+) \approx (1000, 100, 100)$. Figure 3 clearly reflects this process, with vortices appearing in counter-rotating pairs, where the region between the pair induces flow towards the wall, or advects fluid up away from the wall. Downflows carry high-momentum fluid and create high-velocity streaks with $u > 0$ (red contour lines), and the opposite occurs for the upflows, creating slow-velocity streaks with $u < 0$ (blue contour lines). This mechanism is known as 'lift-up' (Brandt, 2014). The results show good agreement between the optimal flow response and the leading SPOD modes for both Reynolds numbers, highlighting that the response to optimal forcing, obtained using the linearized operator, is an accurate model for the leading structures observed in the DNS for the chosen frequency-wavenumber combination, representative of the near-wall cycle.

Agreement between SPOD and resolvent modes

Our aim is to perform additional, detailed quantitative comparisons between the first SPOD mode from the DNS and the optimal response from resolvent analysis. In order to evaluate the agreement for several values of wavelengths λ_x and λ_z at a fixed frequency ω, we define the metric:

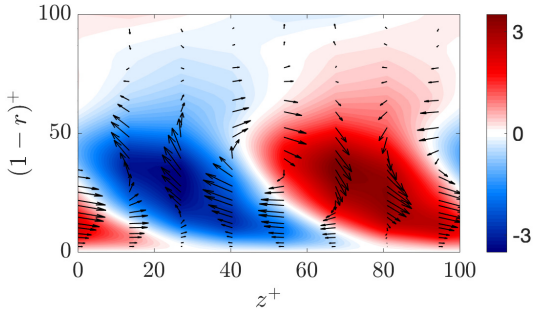

(a) SPOD mode 1

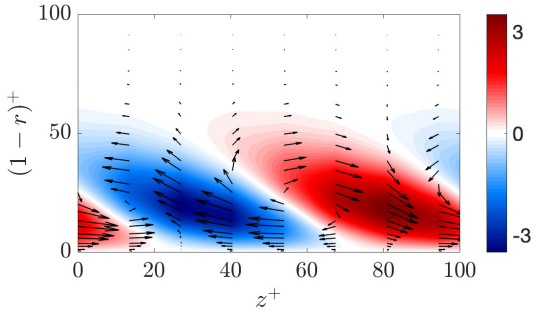

(b) Resolvent mode 1

Figure 3. Comparison between first SPOD mode (a) and optimal response from resolvent analysis (b) using cross-stream view of the $v-w$ components of the vortices (arrows) and the u component of the streak (red and blue contours) for $(\lambda_x^+, \lambda_z^+, \lambda_t^+) \approx (1000, 100, 100)$ at $Re_\tau = 550$.

$$\beta = \frac{\langle \mathbf{q}_{1_{SPOD}}, \mathbf{q}_{1_{res}} \rangle}{||\mathbf{q}_{1_{SPOD}}|| ||\mathbf{q}_{1_{res}}||}, \tag{3}$$

where $\mathbf{q}_{1_{SPOD}}$ is the first SPOD mode, $\mathbf{q}_{1_{res}}$ is the optimal response from resolvent analysis and β is the projection of $\mathbf{q}_{1_{SPOD}}$ into $\mathbf{q}_{1_{res}}$; note that $\langle , \rangle$ denotes inner product. Thus, $\beta = 1$ indicates a perfect alignment between both vectors, and $\beta = 0$ a complete mismatch.

Results of agreement between the first SPOD mode and the optimal response from resolvent analysis in terms of β are shown in Figure 4 (a) for $Re_\tau = 180$ at fixed frequencie $\omega^+ \approx 0.004$; and in Figure 5 (a) for $Re_\tau = 550$ at $\omega^+ \approx 0.006$. The red dashed line in all plots represents the line $\lambda_x^+ = 2\lambda_z^+$, or ratio $\lambda_x^+/\lambda_z^+ = 2$. We can see β close to one for a large part of the parameter space, highlighting a significant region with very good agreement between the first SPOD and resolvent modes, most of it below the line $\lambda_x^+ = 2\lambda_z^+$. The closest agreement ($\beta \approx 1$) is observed for regions with high ratio $\lambda_x^+/\lambda_z^+ > 2$, which corresponds to streaky structures, highlighting that resolvent analysis leads to an accurate modeling of such turbulent structures in turbulent pipe flow.

In order to explore features leading to better or worse agreement (β close to 1 or 0, respectively), we evaluated for both friction Reynolds numbers the ratio of first and second SPOD eigenvalues in logarithmic scale $\log_{10}(\lambda_1/\lambda_2)$, show in Figure 4 (b) for $Re_\tau = 180$ at $\omega^+ \approx 0.004$; and in Figure 5 (b) for $Re_\tau = 550$ at $\omega^+ \approx 0.006$. These results identify the regions where the first SPOD mode is much more energetic than the second mode, leading to a nearly rank-1 behaviour in the DNS cross-spectral density. We can observe regions where the ratio $\log_{10}(\lambda_1/\lambda_2)$ is large, for the wavenumbers with good agreement between the first SPOD and resolvent modes, corresponding to $\beta > 0.8$ (see Figures 4 (a) and 5 (a)); this behavior is observed even for some regions crossing the line $\lambda_x^+ = 2\lambda_z^+$. This thus indicates that regions where the first SPOD mode is much more energetic than the second may be accurately modelled considering the optimal forcing and response from resolvent analysis.

We also evaluated the ratio of optimal and suboptimal resolvent gains in logarithmic scale $\log_{10}(\sigma_1/\sigma_2)$, indicating regions where the optimal gain is much larger than the suboptimal; these results are shown in Figure 4 (c) and Figure 5 (c) at the two analysed Reynolds numbers, for the considered frequencies in the preceding plots. We observe in general that regions where the first resolvent gain is much larger than the second also correspond to the region of good SPOD-resolvent agreement, *i.e.* mostly below the line $\lambda_x^+ = 2\lambda_z^+$.

The analysis above highlights that good agreement between leading SPOD and resolvent modes is observed when a certain mode dominance is verified by analysis of data and/or the linearised operator. We now investigate whether this dominance can be attributed to the lift-up mechanism. The lower triangle delimited by the white line in all plots in Figures 4 and 5 are the streaky reagion, denoting the presence of lift-up effect, at $Re_\tau = 180$ and 550 respectively. This reagion shows an indicator of lift-up mechanism from resolvent analysis. Resolvent modes are here considered to be related to the lift-up effect when the maximum absolute forcing ratio $\max(|f_y|/|f_x|)$, $\max(|f_z|/|f_x|)$ (indicating streamwise vortices as optimal forcing) and the maximum absolute response ratio $\max(|u|/|v|)$, $\max(|u|/|w|)$ (indicating streaks of streamwise velocity as associated most amplified response) are simultaneously larger than 1. We can observe that in regions satisfying these criteria are inside the "lift-up" contour in Figures 4 and 5. The result shows that the regions where the lift-up mechanism is present are essentially the same as those where β is close to 1. Similar results were obtained for higher frequencies, $\omega^+ \approx 0.025$, 0.054 and 0.064. The present results highlight that the lift-up mechanism is active for a wide range of frequencies and wavenumbers in turbulent pipe flow, with a strong amplification mechanism leading to structures that dominate the velocity field.

CONCLUSIONS

In the present study we used signal processing of a DNS, based on SPOD, to identify coherent structures in a turbulent pipe flow for friction Reynolds numbers $Re_\tau = 180$ and 550. In order to model such structures, a theoretical approach, *i.e.* resolvent analysis, was used. The homogeneous directions of this flow allow the evaluation of SPOD and resolvent analysis over a range of streamwise and azimuthal wavenumbers and frequencies. The mean flow was used as a basis for the computation of resolvent modes; optimal responses were considered as the most likely structures to be excited by non-linear terms in the Navier–Stokes system, particularly when the gain of the optimal forcing is much larger than for suboptimal ones (Beneddine *et al.*, 2016; Cavalieri *et al.*, 2019). Coherent structures in the flow were extracted using SPOD, and we carried out thorough quantitative comparisons between leading response modes from the resolvent analysis and the SPOD eigenfunctions.

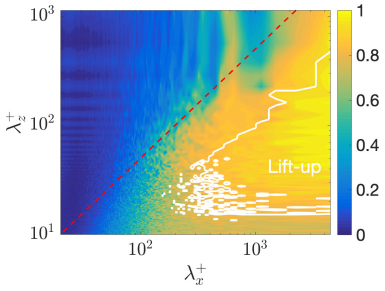

(a) β_1, $\omega^+ \approx 0.004$

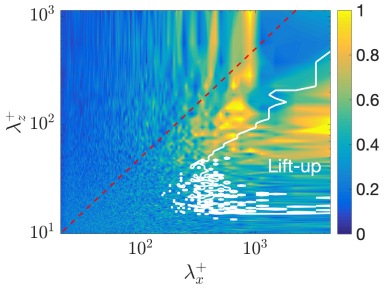

(b) $\log_{10}(\lambda_1/\lambda_2)$, $\omega^+ \approx 0.004$

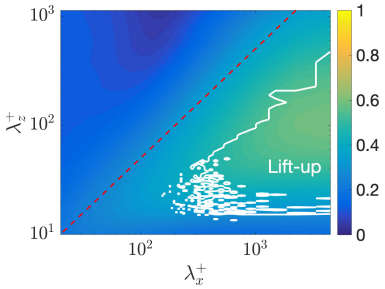

(c) $\log_{10}(\sigma_1/\sigma_2)$, $\omega^+ \approx 0.004$

Figure 4. (a) Agreement between first SPOD and resolvent modes characterized in terms of β. (b) Ratio of first and second SPOD eigenvalues in logarithmic scale. (c) Ratio of optimal and suboptimal resolvent gains in logarithmic scale. Results at $Re_\tau = 180$ for fixed frequencie $\omega^+ \approx 0.004$. The red dashed line in all plots represents the line $\lambda_x^+ = 2\lambda_z^+$. The lower triangle delimited by the white line in all plots are the streaky reagion, denoting the presence of lift-up effect.

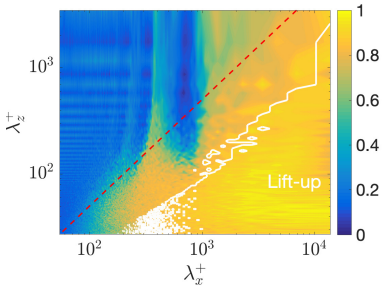

(a) β_1, $\omega^+ \approx 0.006$

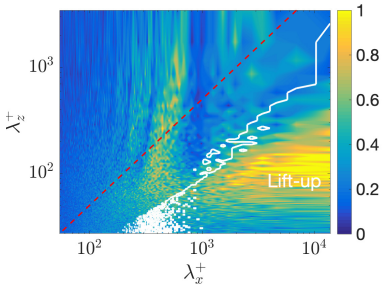

(b) $\log_{10}(\lambda_1/\lambda_2)$, $\omega^+ \approx 0.006$

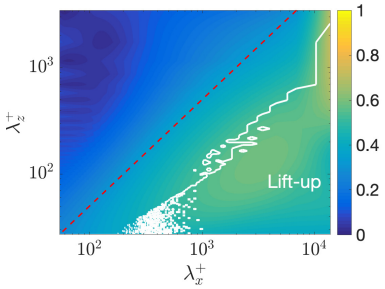

(c) $\log_{10}(\sigma_1/\sigma_2)$, $\omega^+ \approx 0.006$

Figure 5. (a) Agreement between first SPOD and resolvent modes characterized in terms of β. (b) Ratio of first and second SPOD eigenvalues in logarithmic scale. (c) Ratio of optimal and suboptimal resolvent gains in logarithmic scale. Results at $Re_\tau = 550$ for fixed frequencie $\omega^+ \approx 0.006$. The red dashed line in all plots represents the line $\lambda_x^+ = 2\lambda_z^+$. The lower triangle delimited by the white line in all plots are the streaky reagion, denoting the presence of lift-up effect.

For both Reynolds numbers, the results show good agreement between SPOD and resolvent, mostly for $2\lambda_z^+ \leq \lambda_x^+$. These are parameters related to streaky structures, with aspect ratio (streamwise over azimuthal extent) larger than 2. We evaluated the ratio between first and second SPOD eigenvalues, as well the ratio between optimal and suboptimal gain from resolvent analysis, and observed that the regions where those ratios have larger values correspond to cases where the agreement between SPOD and resolvent modes are good.

We also explored the physical reasons behind this agreement by introducing an indicator of the lift-up mechanism using the optimal forcing and associated response from resolvent analysis. Such mechanism is considered as active when forcing is related to streamwise vortices and associated responses to streaks. The results show a clear lift-up effect for wavenumbers and frequencies with good agreement between SPOD and resolvent modes.

In conclusion, based on our results it can be stated that the resolvent analysis provides a simplified model leading to an accurate representation of the streaky structures associated to the lift-up mechanism, particularly for the streamwise velocity. Such structures are observed for a broad range of frequencies and wavenumbers, which indicates that the lift-up effect occurs over a wide range of scales in turbulent pipe flow. It is not surprising to find streamwise vortices leading to streaks in wall-bounded turbulence, since this has been considered as an important part of the dynamics of such flows for some time (Landahl, 1980; Hamilton *et al.*, 1995). The present results highlight the relevance of this mechanism for most of the parameters considered in turbulent pipe flow, which can be understood by the clear dominance of the optimal forcing, with the shape of streamwise vortices, in leading to amplified flow responses of streaky shape. Lift-up thus is naturally selected as the preferred mechanism giving rise to coherent structures in turbulent

pipe flow.

ACKNOWLEDGMENTS

The authors acknowledge the financial support received from Conselho Nacional de Desenvolvimento Científico e Tecnológico, CNPq, under grant No. 310523/2017-6, and by CAPES through the PROEX program. We also acknowledge funding from CISB.

REFERENCES

Abreu, L. I., Cavalieri, A. V. G. & Wolf, W. R. 2017 Coherent hydrodynamic waves and trailing-edge noise. In *23rd AIAA/CEAS Aeroacoustics Conference*, p. 3173.

Beneddine, S., Sipp, D., Arnault, A., Dandois, J. & Lesshafft, L. 2016 Conditions for validity of mean flow stability analysis. *Journal of Fluid Mechanics* **798**, 485–504.

Brandt, L. 2014 The lift-up effect: the linear mechanism behind transition and turbulence in shear flows. *European Journal of Mechanics-B/Fluids* **47**, 80–96.

Cavalieri, A.V.G., Jordan, P. & Lesshafft, L. 2019 Wave-packet models for jet dynamics and sound radiation. *Applied Mechanics Reviews* **71** (2), 020802.

El Khoury, G.K., Schlatter, P., Noorani, A., Fischer, P.F., Brethouwer, G. & Johansson, A.V. 2013 Direct numerical simulation of turbulent pipe flow at moderately high reynolds numbers. *Flow, Turbulence and Combustion* **91** (3), 475–495.

Gómez, F., Blackburn, H.M., Rudman, M., McKeon, B.J., Luhar, M., Moarref, R. & Sharma, A.S. 2014 On the origin of frequency sparsity in direct numerical simulations of turbulent pipe flow. *Physics of Fluids* **26** (10), 101703.

Gupta, A.K., Laufer, J. & Kaplan, R.E. 1971 Spatial structure in the viscous sublayer. *Journal of Fluid Mechanics* **50** (3), 493–512.

Hamilton, J.M., Kim, J. & Waleffe, F. 1995 Regeneration mechanisms of near-wall turbulence structures. *Journal of Fluid Mechanics* **287**, 317–348.

Hellström, L.H.O., Marusic, I. & Smits, A.J. 2016 Self-similarity of the large-scale motions in turbulent pipe flow. *Journal of Fluid Mechanics* **792**.

Hoyas, S. & Jiménez, J. 2006 Scaling of the velocity fluctuations in turbulent channels up to Re_τ= 2003. *Physics of Fluids* **18** (1), 011702.

Jiménez, J. 2013 Near-wall turbulence. *Physics of Fluids* **25** (10), 101302.

Jovanovic, M.R. & Bamieh, B. 2005 Componentwise energy amplification in channel flows. *Journal of Fluid Mechanics* **534**, 145–183.

Kline, S. J., Reynolds, W. C., Schraub, F. A. & Runstadler, P. W. 1967 The structure of turbulent boundary layers. *Journal of Fluid Mechanics* **30** (4), 741–773.

Landahl, M.T. 1980 A note on an algebraic instability of inviscid parallel shear flows. *Journal of Fluid Mechanics* **98** (2), 243–251.

Marusic, I., Baars, W.J. & Hutchins, N. 2017 Scaling of the streamwise turbulence intensity in the context of inner-outer interactions in wall turbulence. *Physical Review Fluids* **2** (10), 100502.

McKeon, B.J. 2017 The engine behind (wall) turbulence: perspectives on scale interactions. *Journal of Fluid Mechanics* **817**.

McKeon, B. J. & Sharma, A. S. 2010 A critical-layer framework for turbulent pipe flow. *Journal of Fluid Mechanics* **658**, 336–382.

Monty, JP, Hutchins, N, Ng, HCH, Marusic, I & Chong, MS 2009 A comparison of turbulent pipe, channel and boundary layer flows. *Journal of Fluid Mechanics* **632**, 431–442.

Towne, A., Schmidt, O.T. & Colonius, T. 2018 Spectral proper orthogonal decomposition and its relationship to dynamic mode decomposition and resolvent analysis. *Journal of Fluid Mechanics* **847**, 821867.